Applied Physics Letters ARTICLE scitation.org/journal/apl

Curvature-driven homogeneous Dzyaloshinskii–Moriya interaction and emergent weak ferromagnetism in anisotropic antiferromagnetic spin chains

Cite as: Appl. Phys. Lett. **118**, 182405 (2021); doi: 10.1063/5.0048823
Submitted: 26 February 2021 · Accepted: 9 April 2021 ·
Published Online: 4 May 2021

Oleksandr V. Pylypovskyi,[1,2] Yelyzaveta A. Borysenko,[3] Jürgen Fassbender,[1] Denis D. Sheka,[3] and Denys Makarov[1,a)]

AFFILIATIONS

[1]Helmholtz-Zentrum Dresden-Rossendorf e.V., Institute of Ion Beam Physics and Materials Research, 01328 Dresden, Germany
[2]Kyiv Academic University, 03142 Kyiv, Ukraine
[3]Taras Shevchenko National University of Kyiv, 01601 Kyiv, Ukraine

Note: This paper is part of the APL Special Collection on Mesoscopic Magnetic Systems: From Fundamental Properties to Devices.
[a)]**Author to whom correspondence should be addressed:** d.makarov@hzdr.de

ABSTRACT

Chiral antiferromagnets are currently considered for a broad range of applications in spintronics, spin-orbitronics, and magnonics. In contrast to the established approach relying on materials screening, the anisotropic and chiral responses of low-dimensional antiferromagnets can be tailored relying on the geometrical curvature. Here, we consider an achiral, anisotropic antiferromagnetic spin chain and demonstrate that these systems possess geometry-driven effects stemming not only from the exchange interaction but also from the anisotropy. Peculiarly, the anisotropy-driven effects are complementary to the curvature effects stemming from the exchange interaction and rather strong as they are linear in curvature. These effects are responsible for the tilt of the equilibrium direction of vector order parameters and the appearance of the homogeneous Dzyaloshinskii–Moriya interaction. The latter is a source of the geometry-driven weak ferromagnetism emerging in curvilinear antiferromagnetic spin chains. Our findings provide a deeper fundamental insight into the physics of curvilinear antiferromagnets beyond the σ-model and offer an additional degree of freedom in the design of spintronic and magnonic devices.

Antiferromagnets (AFMs) represent a rich class of technologically promising materials, whose magnetic properties are determined by the antiparallel configuration of neighboring spins.[1–4] One of the distinct properties of AFMs is related to the variety of intrinsic crystal symmetries and mechanisms of the exchange[5] and anisotropy.[5,6] Within the phenomenological formalism, this is reflected in the specific energy invariants, mixing components of different vector order parameters.[7] In this way, Dzyaloshinskii–Moriya interaction (DMI) in AFMs appears in two distinct forms. The so-called homogeneous DMI links ferromagnetic and staggered order parameters and does not contain their spatial derivatives. The homogeneous DMI is responsible for the anisotropic responses and weak ferromagnetism. The inhomogeneous DMI described by the Lifshits invarians and also characteristic for ferromagnets determines the appearance of non-collinear and incommensurable magnetic textures.[7–9] Among them, antiferromagnetic chiral domain walls and skyrmions are perspective information carriers[2] and functional elements of prospective devices.[10,11] Microscopically, the local break of the inversion symmetry leads to the DMI[12,13] and staggered spin–orbit torques.[14] This enables an efficient interaction between the electrical current and magnetic textures, resulting in ultrahigh velocities of magnetic solitons.[15,16] In addition to the intrinsic properties of the crystal lattice, the magnetic responses can be tuned by the geometry of the samples, which allows us to utilize boundary conditions[17,18] and geometrical curvatures to design non-collinear magnetic states[19] and dispersion curves.[20]

In this work, we develop the analytical approach beyond the σ-model to describe curvilinear one-dimensional (1D) AFMs and determine conditions when they possess the geometry-driven weak

ferromagnetism. We show that in contrast to ferromagnets (FMs), AFMs exhibit the geometry-driven modification of the magnetic responses stemming not only from the exchange but also from the anisotropy interaction. The key consequences of the fact that the anisotropy axis follows the shape of the spin chain are the appearance of the homogeneous DMI energy term and the tilt of the anisotropy axis in the osculating plane. These effects originate from the multiplicity of magnetic sublattices in AFMs. Therefore, our results are of importance for curvilinear ferrimagnetic systems as well.

We consider intrinsically achiral, anisotropic antiferromagnetic spin chains with the Hamiltonian $\mathscr{H} = \mathscr{H}_{\rm x} + \mathscr{H}_{\rm a} + \mathscr{H}_{\rm f}$, where $\mathscr{H}_{\rm x}$ represents the nearest-neighbor exchange, $\mathscr{H}_{\rm a}$ is the anisotropic part of the Hamiltonian, and $\mathscr{H}_{\rm f}$ is the interaction with the external magnetic field $\boldsymbol{H}$. The magnetic moments $\boldsymbol{M}_i$ with $i = \overline{0, N-1}$ and N being the total number of spins are arranged along a space curve $\boldsymbol{\gamma}(s)$ with s being the arc length. The geometrical properties of $\boldsymbol{\gamma}$ are determined[21] by the curvature, $\kappa(s) = |\boldsymbol{\gamma}' \times \boldsymbol{\gamma}''|$, and torsion $\tau(s) = [\boldsymbol{\gamma}' \times \boldsymbol{\gamma}''] \cdot \boldsymbol{\gamma}''' / |\boldsymbol{\gamma}''|^2$, where prime indicates the derivative with respect to s. The local reference frame is determined by the tangential $\boldsymbol{e}_{\rm T} = \boldsymbol{\gamma}'$, normal $\boldsymbol{e}_{\rm N} = \boldsymbol{\gamma}''/\kappa$ and binormal $\boldsymbol{e}_{\rm B} = \boldsymbol{e}_{\rm T} \times \boldsymbol{e}_{\rm N}$ directions, respectively. In the following, we discuss weakly curved geometries, i.e., $\kappa, |\tau| \ll 1/\ell \ll 1/a_0$, where ℓ is the magnetic length, determined by the competition between the exchange and anisotropy interactions, a_0 is the lattice constant. We assume that the system is far below the Néel temperature and all magnetic moments are of a constant length $M_0 = 2\mu_{\rm B} S$ with $\mu_{\rm B}$ being the Bohr magneton and S being the spin length.

The nearest-neighbor antiferromagnetic exchange $\mathscr{H}_{\rm x} = (\mathscr{J} S^2/2) \sum_i \boldsymbol{\mu}_i \cdot \boldsymbol{\mu}_{i+1}$ with the exchange integral $\mathscr{J} > 0$ and $\boldsymbol{\mu}_i = \boldsymbol{M}_i/M_0$ allows us to identify two sublattices of magnetic moments and introduce staggered (Néel) and ferromagnetic vector order parameters, $\boldsymbol{n}_i = (\boldsymbol{\mu}_{2i} - \boldsymbol{\mu}_{2i+1})/2$ and $\boldsymbol{m}_i = (\boldsymbol{\mu}_{2i} + \boldsymbol{\mu}_{2i+1})/2$, respectively. The micromagnetic exchange energy reads

$$E_{\rm x} = \int w_{\rm x}\, {\rm d}s, \qquad w_{\rm x} = \Lambda m^2 + A_0(\boldsymbol{n}'^2 - \boldsymbol{m}'^2) + \lambda \boldsymbol{m} \cdot \boldsymbol{n}', \tag{1}$$

where $\boldsymbol{n}$ and $\boldsymbol{m}$ are the continuum counterparts of $\boldsymbol{n}_i$ and $\boldsymbol{m}_i$, respectively, the constant of the uniform exchange $\Lambda = 2\mathscr{J} S^2/a_0$, exchange stiffness $A_0 = \mathscr{J} S^2 a_0$ and $\lambda = 2\mathscr{J} S^2$; see the supplementary material for details. The latter term with the parity breaking coefficient λ lifts the degeneracy of energy with respect to the dimerization of the AFM chain.[22–24] It renormalizes the exchange stiffness $A = A_0/2$ within the σ-model and leads to the intrinsic magnetization of non-uniform textures.[24] The expression (1) is similar to the exchange energy of 1D AFMs[24] with the difference that the spatial derivatives are taken in the curvilinear reference frame. The curvature effects stemming from the exchange term $\boldsymbol{n}'^2$ are discussed in Ref. 20. The term $\boldsymbol{m}'^2$ is expected to affect the system near the spin-flip transition. As we will show in the following, the parity breaking term in (1) scales linearly with κ and τ and is a source of the weak ferromagnetism in curvilinear AFM spin chains.

The anisotropic contribution to the microscopic Hamiltonian can be presented by the so-called inter-ion and single-ion anisotropies;[25] see Fig. 1(a). In the simplest case of one symmetry axis $\boldsymbol{e}_{\rm a}$ at the position of the i-th spin, the anisotropic part of the Hamiltonian reads

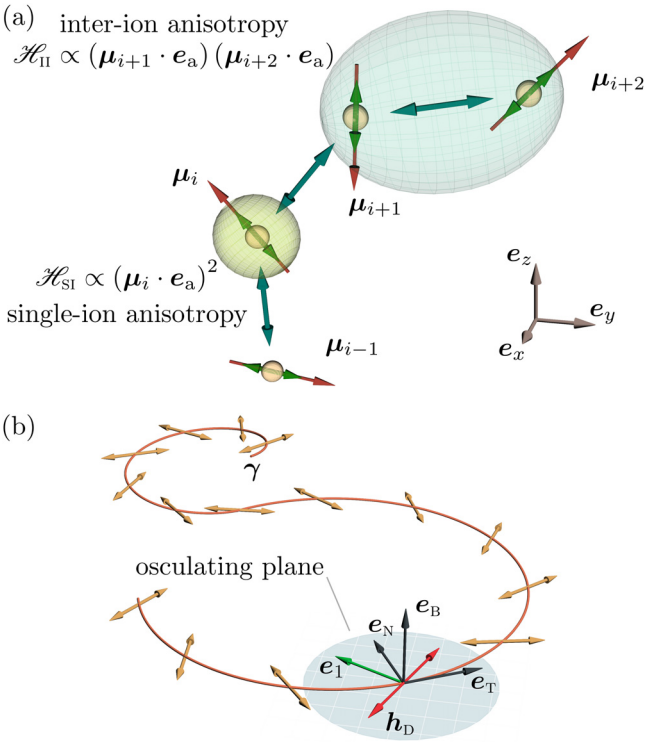

FIG. 1. Anisotropic antiferromagnetic spin chain: (a) spin chain with unit vectors of magnetic moments $\boldsymbol{\mu}_i$ (red arrows). Double arrows (green) show the anisotropy axes of the single- and inter-ion anisotropies for the given magnetic sites $\mathscr{H}_{\rm SI}$ and $\mathscr{H}_{\rm II}$, respectively. (b) Micromagnetic representation of the spin chain along the curve $\boldsymbol{\gamma}$ with $\boldsymbol{n}$ being the Néel vector. The local TNB reference frame is indicated with black arrows. Vector $\boldsymbol{h}_{\rm D}$ represents the effective field of the longitudinal homogeneous DMI. The arrow $\boldsymbol{e}_1$ shows the equilibrium direction of the anisotropy axes due to the interplay between $w_{\rm a}$ and $\tilde{w}_{\rm a}$.

$$\mathscr{H}_{\rm a} = -\frac{\mathscr{K}_{\rm SI} S^2}{2} \sum_i (\boldsymbol{\mu}_i \cdot \boldsymbol{e}_{\rm a})^2 + \frac{\mathscr{K}_{\rm II} S^2}{2} \sum_i (\boldsymbol{\mu}_i \cdot \boldsymbol{e}_{\rm a})(\boldsymbol{\mu}_{i+1} \cdot \boldsymbol{e}_{\rm a}). \tag{2}$$

The first term represents the single-ion anisotropy with the constant $\mathscr{K}_{\rm SI}$, which is determined by the spin–orbit interaction and is relevant for $S \geq 1$.[5,25] The second term determines the inter-ion anisotropic interactions with the anisotropy constant $\mathscr{K}_{\rm II}$, originating from the anisotropic exchange interaction, spin–orbit interaction, and dipolar interaction.[5,25] Micromagnetically, single-ion and inter-ion anisotropies have different contributions to the characteristic magnetic fields of the phase transitions.[25] If the dipolar interaction has no other competing anisotropic terms (the case of an isotropic AFM with dipolar interaction), it leads to the hard-axis anisotropy with $\boldsymbol{e}_{\rm a} = \boldsymbol{e}_{\rm T}$.[20]

In the following, we limit ourselves by the case of the tangential direction of the anisotropy axis, $\boldsymbol{e}_{\rm a} = \boldsymbol{e}_{\rm T}$. In this case, the micromagnetic expression for the anisotropy energy reads

$$E_{\rm a} = \int \left(w_{\rm a} + w_{\rm pb} + \tilde{w}_{\rm a} + w_{\rm D}\right) {\rm d}s, \qquad w_{\rm a} = -K_n n_{\rm T}^2 - K_m m_{\rm T}^2, \quad w_{\rm pb} = \lambda_{\rm T} m_{\rm T} n_{\rm T}', \qquad \tilde{w}_{\rm a} = -\tilde{K}_n n_{\rm T} n_{\rm N} - \tilde{K}_m m_{\rm T} m_{\rm N}, \quad w_{\rm D} = \boldsymbol{h}_{\rm D} \cdot \boldsymbol{m}. \tag{3}$$

Here, the first term w_a with $K_{n,m} = (\mathscr{K}_{SI} \pm \mathscr{K}_{II})S^2/(2a_0)$ represents the regular micromagnetic anisotropy, also present in straight spin chains with the given easy axis $\boldsymbol{e}_a$. The term w_{pb} in (3) with $\lambda_T = \mathscr{K}_{II}S^2$ introduces anisotropy into the exchange-driven parity breaking term. Other terms are determined by the geometrical parameters of $\boldsymbol{\gamma}$; see Fig. 1(b).

The emergent homogeneous (longitudinal) DMI term w_D indicates the presence of a weak ferromagnetism-like contribution with the Dzyaloshinskii effective field $\boldsymbol{h}_D = D_{SI}(n_N \boldsymbol{e}_T + n_T \boldsymbol{e}_N)$ and $D_{SI} = \kappa \mathscr{K}_{SI} S^2/2$. These energy invariants can be present in crystals with 2_z or σ_z symmetry if $\boldsymbol{e}_z$ axis is associated with the tangential direction[26] and are responsible for the nonlinearity of AFM resonance.[27] The contribution of this term can be expected for any curve with $\kappa \neq 0$ if the AFM texture possesses the tangential and (or) normal components of $\boldsymbol{n}$. In flat systems $\boldsymbol{n} = \boldsymbol{e}_B$, which leads to $\boldsymbol{h}_D = 0$. In contrast, in space curves, the normal and binormal components of $\boldsymbol{n}$ are present, e.g., in the homogeneous ground state of an AFM helix;[20] see Fig. 2(a). The strength of $\boldsymbol{h}_D$ increases with torsion and curvature and can reach up to about 10% of the anisotropy field [Fig. 2(b)]. Alternatively, the homogeneous DMI field can be enhanced by orders of magnitude at the location non-collinear AFM textures, such as Bloch or Néel domain walls; see Fig. 2(c). We note that this enhancement of the $\boldsymbol{h}_D$ at the location of non-collinear textures is due to the non-zero magnetization of the domain wall in a 1D system.[24,28] The finite magnetization at the texture location makes the contribution of the w_D term significant.

The term $\tilde{w}_a$ with $\tilde{K}_{n,m} = \kappa(\mathscr{K}_{SI} \pm \mathscr{K}_{II})S^2/2$ represents the non-diagonal components of the total anisotropy tensor contributing to the energy in addition to the geometry-driven anisotropy stemming from the exchange interaction. Note that the latter one is scaled as $\kappa\tau$ and absent in flat curves[20] in contrast to $\tilde{w}_a \propto \kappa$; see Fig. 3(a). The equilibrium direction of the anisotropy axes is determined by the diagonal form of the anisotropy tensor. The tilt ψ of the easy axis from $\boldsymbol{e}_N$ in the case of an AFM ring is shown in Fig. 3(b).

The interaction of the spin chain with the uniform external magnetic field $\boldsymbol{H}$ is described by $\mathscr{H}_f = -M_0 \sum_i \boldsymbol{\mu}_i \cdot \boldsymbol{H}$. The macroscopic Lagrangian, allowing us to determine the equations of motion for the vector order parameters reads $L = -2M_s/\gamma_0 \int \boldsymbol{m} \cdot [\boldsymbol{n} \times \dot{\boldsymbol{n}}] ds - E_{tot}$ with the total energy $E_{tot} = E_x + E_a + E_f = \int w_{tot} ds$, where γ_0 is the gyromagnetic ratio, the dot indicates the derivative with respect to time, $M_s = M_0/(2a_0)$ is the saturation magnetization of one sublattice, and $E_f = -2M_s \int \boldsymbol{m} \cdot \boldsymbol{H} ds$ is the energy of the interaction with the magnetic field. We limit the following discussion by the case of a strong intrinsic anisotropy with the hard axis along $\boldsymbol{e}_T$. Then, the magnetic length reads $\ell = \sqrt{A_0/(2|K_n|)}$, where $K_n < 0$. For the magnetic fields smaller than or comparable to the spin-flop field, the magnetization of the ring is small enough, which allows us to apply a standard variational approach for the Lagrangian to determine the relation between $\boldsymbol{n}$ and $\boldsymbol{m}$ in equilibrium. Taking into account that $\boldsymbol{m} \cdot \boldsymbol{n} = 0$ and $n^2 + m^2 = 1$, the magnetization reads

$$\boldsymbol{m} \approx -\varsigma \boldsymbol{n} \times \left[\omega_0 \dot{\boldsymbol{n}} + (\ell \boldsymbol{n}' - \boldsymbol{H}/H_0) \times \boldsymbol{n}\right], \tag{4}$$

where $\varsigma = a_0/(2\ell)$ is the expansion parameter measuring the strength of the effective anisotropy field with respect to the exchange field, $H_0 = \sqrt{\Lambda K_n}/M_s$ is the characteristic magnetic field, and $\omega_0 = \gamma_0 H_0$ is the characteristic frequency. The term

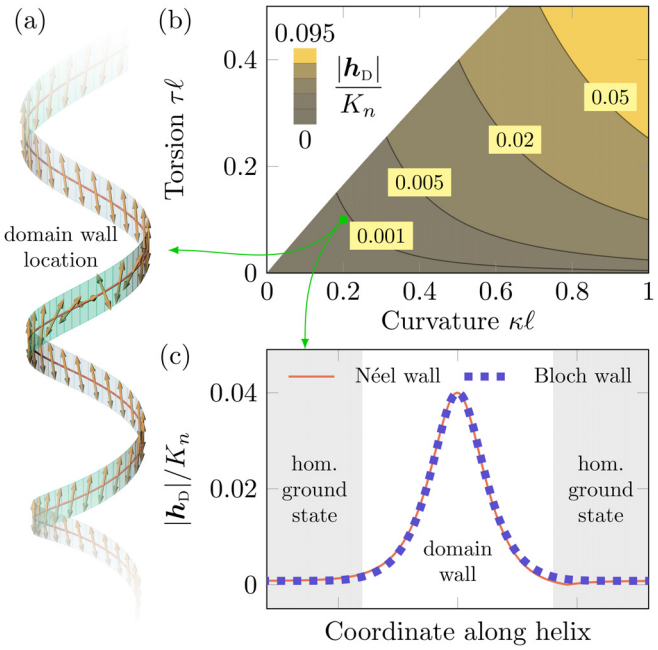

FIG. 2. Curvature-driven homogeneous DMI. Domain wall in an AFM helix. (b) The homogeneous Dzyaloshinskii field $|\boldsymbol{h}_D|$ for the case of the homogeneous ground state[20] of the helical spin chain in the absence of the inter-ion anisotropy ($\varsigma = 0.1$). The white region corresponds to the periodic ground state.[20] (c) $|\boldsymbol{h}_D|$ for Bloch and Néel domain walls on a helical spin chain ($\kappa\ell = 0.2$, $\tau\ell = 0.1$, $\varsigma = 0.1$). The region with the ground state of $\boldsymbol{n}$ is highlighted in gray.

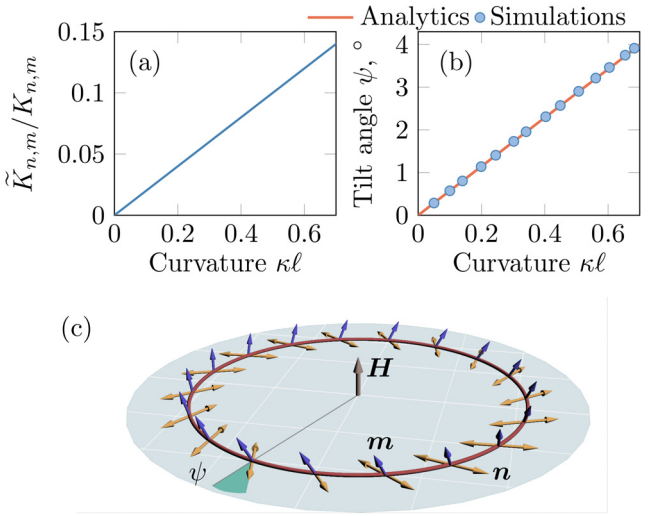

FIG. 3. Curvature-driven tilt of the anisotropy axis. (a) Relative strength of the geometry-driven anisotropic term, which is proportional to the curvature ($\mathscr{K}_{II}/\mathscr{K}_{SI} = 0.3$, $\varsigma = 0.1$). (b) Tilt angle of the anisotropy axis as a function of curvature ($\mathscr{K}_{II} = 0$, $\varsigma = 0.1$). (c) AFM ring exposed to an external magnetic field $\boldsymbol{H}$ applied perpendicular to the ring plane. In equilibrium, the direction ψ of $\boldsymbol{n}$ coincides with the tilted anisotropy axis shown in panel (b).

TABLE I. Comparison of geometry-driven responses in FM and AFM spin chains. The exchange interaction contributes to the geometry-driven anisotropy and inhomogeneous DMI in both, FMs and AFMs. A variety of sources of anisotropy and multiple vector order parameters lead to the appearance of the geometry-driven anisotropic response and homogeneous DMI of longitudinal symmetry in AFM spin chains. Curvature-driven effects stemming from the anisotropy interaction are absent in FM spin chains.

	Curvature-driven response in		
	anisotropy	hom. DMI	inhom. DMI
Exchange	FM and AFM	✗	FM and AFM
Anisotropy	AFM	AFM	✗

$$\boldsymbol{n}' = (n'_{\mathrm{T}} - \kappa n_{\mathrm{N}})\boldsymbol{e}_{\mathrm{T}} + (n'_{\mathrm{N}} + \kappa n_{\mathrm{T}} - \tau n_{\mathrm{B}})\boldsymbol{e}_{\mathrm{N}} + (n'_{\mathrm{B}} + \tau n_{\mathrm{N}})\boldsymbol{e}_{\mathrm{B}}. \quad (5)$$

Eq. (4) originates from the parity breaking term in the expression for the exchange energy (1). This is a source of the weak ferromagnetism in curvilinear AFM spin chains, which is manifested by the presence of a non-zero radial magnetization. Based on (4), for the weakly curved spin chains supporting homogeneous textures in the TNB reference frame, the magnetization reads $\boldsymbol{m} = \varsigma\ell[\kappa n_{\mathrm{N}}\boldsymbol{e}_{\mathrm{T}} + (\tau n_{\mathrm{B}} - \kappa n_{\mathrm{T}})\boldsymbol{e}_{\mathrm{N}} - \tau n_{\mathrm{N}}\boldsymbol{e}_{\mathrm{B}}]$. Therefore, for any spin chain arranged along either a planar curve $\boldsymbol{\gamma}$ with $\boldsymbol{n} \neq \boldsymbol{e}_{\mathrm{B}}$ or a space curve, the system will reveal a weak ferromagnetic response. The strength of the weak ferromagnetism is determined by the curvature and torsion.

The discussed here curvature effects from anisotropy are weaker than those from exchange. Therefore, to explore them, in the following, we identify a system where these effects are pronounced and drive the response of the system. For instance, it is insightful to consider a ring geometry $\boldsymbol{\gamma} = R\{\cos(s/R), \sin(s/R), 0\}$, which implies constant curvature $\kappa = 1/R$ and $\tau = 0$. In this case, the exchange-driven chiral effects are not active and the ground state $\boldsymbol{n} = \boldsymbol{e}_{\mathrm{B}}$ is determined by the exchange-driven easy-axis anisotropy with the coefficient $K_{\mathrm{x}} = \kappa^2 A$.[20] Being exposed to a magnetic field applied along the ring axis, $\boldsymbol{H} = H\boldsymbol{e}_z$, the spin chain experiences the spin-flop transition at the spin-flop field $H_{\mathrm{sf}} = \kappa\sqrt{\Lambda A}/M_{\mathrm{s}}$. This leads to the reorientation of the $\boldsymbol{n}$ to the direction, which is perpendicular to the external field; see Fig. 3(c). The energy of such a planar configuration of the Néel vector $\boldsymbol{n} = \cos\phi\boldsymbol{e}_{\mathrm{T}} + \sin\phi\boldsymbol{e}_{\mathrm{N}}$

$$\frac{w_{\mathrm{tot}}}{K_n} = \underbrace{\ell^2(\kappa + \phi')^2}_{w_{\mathrm{x}}} + \underbrace{\cos^2\phi}_{w_{\mathrm{a}}} + \underbrace{2\varsigma\kappa\ell\sin\phi\cos\phi}_{\tilde{w}_{\mathrm{a}}} - \frac{H^2}{H_0^2}. \quad (6)$$

The equilibrium direction of the Néel vector in the spin-flop phase is determined by the competition between the contributions of the intrinsic hard axis anisotropy oriented along the tangential direction in w_{a} and the curvature-driven non-diagonal term $\tilde{w}_{\mathrm{a}}$. This is the curvature effect stemming from the anisotropy interaction. The minimization of E_{tot} with respect to $\phi(s)$ leads to a uniform, tilted texture in the local reference frame $\phi = \pm\pi/2 + \psi$, where the tilt angle reads

$$\psi \approx \varsigma\kappa\ell, \quad \kappa\ell \ll 1. \quad (7)$$

A comparison of the theoretical prediction (7) with spin–lattice simulations using the in-house developed code SLaSi[29] is shown in Fig. 3(b); see the supplementary material for details. The equilibrium direction of the magnetization $\boldsymbol{m}$ according to (4) reads

$$\boldsymbol{m} \approx \varsigma\left(\frac{\boldsymbol{H}}{H_0} \pm \kappa\ell\boldsymbol{e}_{\mathrm{T}}\right). \quad (8)$$

The tilt of magnetization in the tangential direction is the consequence of the parity breaking term in (1). Different signs in (8) correspond to the energetically degenerate vortex states of the fundamental homotopy group $\pi_1(\mathbb{S}^1)$ with the opposite chiralities (clockwise and counterclockwise).

It is instructive to compare the modification of the geometry-driven responses in FMs and AFMs; see Table I. The geometry-driven chiral and anisotropic responses for the case of intrinsically achiral FM spin chains originate from the exchange interaction.[30] They lead to the tilt of the principal axes of anisotropy[31,32] and chiral responses described by the energy invariants in the form of the inhomogeneous DMI.[31–33] In the intrinsically achiral AFM spin chains, the chiral helimagnetism originates from the nearest-neighbor exchange.[20] The interaction, which is tracking the sample geometry in isotropic FMs, is the magnetostatics leading to the uniaxial anisotropy with the easy axis along the tangential direction $\boldsymbol{e}_{\mathrm{T}}$.[34] In AFMs, the dipolar interaction leads to the hard axis $\boldsymbol{e}_{\mathrm{T}}$,[20] which makes other anisotropic contributions (even if they are weak) to the Hamiltonian pronounced. The latter leads to the appearance of the anisotropic and weakly ferromagnetic responses in curvilinear AFMs, stemming from the single- and inter-ion anisotropies on the level of the spin Hamiltonian.

In summary, we develop an approach beyond the σ-model to analyze curvilinear antiferromagnetism in the intrinsically achiral anisotropic spin chains. We identify the conditions of the presence of the weak ferromagnetism in a curvilinear AFM spin chain and determine the contribution to the geometry-driven magnetic responses stemming from the anisotropy interaction, which are specific to AFM materials. The latter emerges due to the presence of two vector order parameters (ferromagnetic and staggered one) in contrast to FMs and is determined by the local curvature κ of the chain. Thus, the geometry-driven effects stemming from the anisotropy interaction should be pronounced even for flat curvilinear antiferro- and ferrimagnetic architectures. Considering two general microscopic models of anisotropy, namely, single- and inter-ion anisotropies where the anisotropy hard axis is assumed to be along the tangential direction, we quantify the tilt of the principal axes of anisotropy and identify the appearance of the geometry-driven homogeneous DMI energy term and the additional contribution to the parity breaking coefficient. This work opens up an additional route to control AFM textures in spintronic, spin-orbitronics, and magnonic devices relying on the geometrical curvature. In particular, the perspective platforms are atom-by-atom tailored nanomagnets[35–37] and molecular magnets (e.g., wheels with AFM coupling[38,39]).

See the supplementary material for details of analytical derivation of the micromagnetic model from spin–lattice Hamiltonian, spin–lattice simulations, and notes on the intrinsic magnetization of curvilinear AFM spin chains.

We thank Dr. Kostiantyn V. Yershov (IFW Dresden) for fruitful discussions. Spin–lattice simulations were made at the Cluster of Taras Shevchenko National University of Kyiv.[40] This work was financed, in part, via the German Research Foundation (DFG) Grant Nos. MA 5144/22-1, MC 9/22-1, and MA 5144/24-1, Alexander von Humboldt Foundation (Research Group Linkage

Programme), and by the Ministry of Education and Science of Ukraine (Project No. 19BF052-01) and the National Research Foundation of Ukraine Grant (No. 2020.02/0051).

DATA AVAILABILITY

The data that support the findings of this study are available from the corresponding author upon reasonable request.

REFERENCES

[1]O. Gomonay, T. Jungwirth, and J. Sinova, "Concepts of antiferromagnetic spintronics," Phys. Status Solidi RRL **11**, 1700022 (2017).
[2]O. Gomonay, V. Baltz, A. Brataas, and Y. Tserkovnyak, "Antiferromagnetic spin textures and dynamics," Nat. Phys. **14**, 213–216 (2018).
[3]V. Baltz, A. Manchon, M. Tsoi, T. Moriyama, T. Ono, and Y. Tserkovnyak, "Antiferromagnetic spintronics," Rev. Mod. Phys. **90**, 015005 (2018).
[4]Z. Liu, Z. Feng, H. Yan, X. Wang, X. Zhou, P. Qin, H. Guo, R. Yu, and C. Jiang, "Antiferromagnetic piezospintronics," Adv. Electron. Mater. **5**, 1900176 (2019).
[5]E. A. Turov, A. V. Kolchanov, V. V. Menshenin, I. F. Mirsayev, and V. V. Nikolaev, *Symmetry and Physical Properties of Antiferromagnets* (FIZMATLIT, Moscow, 2001).
[6]K. O'Grady, J. Sinclair, K. Elphick, R. Carpenter, G. Vallejo-Fernandez, M. I. J. Probert, and A. Hirohata, "Anisotropy in antiferromagnets," J. Appl. Phys. **128**, 040901 (2020).
[7]Y. A. Izyumov, "Modulated, or long-periodic, magnetic structures of crystals," Sov. Phys. Usp. **27**, 845 (1984).
[8]A. N. Bogdanov and D. A. Yablonskiĭ, "Thermodynamically stable "vortices" in magnetically ordered crystals. The mixed state of magnets," J. Exp. Theor. Phys. **68**, 101 (1989) [Zh. Exp. Teor. Fiz. **95**, 178 (1989)]; available at http://jetp.ac.ru/cgi-bin/e/index/e/68/1/p101?a=list
[9]A. N. Bogdanov, U. K. Rößler, M. Wolf, and K.-H. Müller, "Magnetic structures and reorientation transitions in noncentrosymmetric uniaxial antiferromagnets," Phys. Rev. B **66**, 214410 (2002).
[10]L. Shen, J. Xia, G. Zhao, X. Zhang, M. Ezawa, O. A. Tretiakov, X. Liu, and Y. Zhou, "Spin torque nano-oscillators based on antiferromagnetic skyrmions," Appl. Phys. Lett. **114**, 042402 (2019).
[11]L. Shen, J. Xia, X. Zhang, M. Ezawa, O. A. Tretiakov, X. Liu, G. Zhao, and Y. Zhou, "Current-induced dynamics and chaos of antiferromagnetic bimerons," Phys. Rev. Lett. **124**, 037202 (2020).
[12]I. Dzyaloshinsky, "A thermodynamic theory of 'weak' ferromagnetism of antiferromagnetics," J. Phys. Chem. Solids **4**, 241–255 (1958).
[13]T. Moriya, "Anisotropic superexchange interaction and weak ferromagnetism," Phys. Rev. **120**, 91–98 (1960).
[14]J. Železný, H. Gao, K. Výborný, J. Zemen, J. Mašek, A. Manchon, J. Wunderlich, J. Sinova, and T. Jungwirth, "Relativistic Néel-order fields induced by electrical current in antiferromagnets," Phys. Rev. Lett. **113**, 157201 (2014).
[15]J. Barker and O. A. Tretiakov, "Static and dynamical properties of antiferromagnetic skyrmions in the presence of applied current and temperature," Phys. Rev. Lett. **116**, 147203 (2016).
[16]O. Gomonay, T. Jungwirth, and J. Sinova, "High antiferromagnetic domain wall velocity induced by Néel spin-orbit torques," Phys. Rev. Lett. **117**, 017202 (2016).
[17]N. Hedrich, K. Wagner, O. V. Pylypovskyi, B. J. Shields, T. Kosub, D. D. Sheka, D. Makarov, and P. Maletinsky, "Nanoscale mechanics of antiferromagnetic domain walls," Nat. Phys. (unpublished).
[18]O. V. Pylypovskyi, A. V. Tomilo, D. D. Sheka, J. Fassbender, and D. Makarov, "Boundary conditions for the Néel order parameter in a chiral antiferromagnetic slab," Phys. Rev. B **103**, 134413 (2021).
[19]S. Castillo-Sepúlveda, R. A. Escobar, D. Altbir, M. Krizanac, and E. Y. Vedmedenko, "Magnetic Möbius stripe without frustration: Noncollinear metastable states," Phys. Rev. B **96**, 024426 (2017).
[20]O. V. Pylypovskyi, D. Y. Kononenko, K. V. Yershov, U. K. Rößler, A. V. Tomilo, J. Fassbender, J. van den Brink, D. Makarov, and D. D. Sheka, "Curvilinear one-dimensional antiferromagnets," Nano Lett. **20**, 8157–8162 (2020).
[21]W. Kühnel, *Differential Geometry: Curves—Surfaces—Manifolds* (American Mathematical Society, 2015).
[22]B. A. Ivanov and A. K. Kolezhuk, "Solitons in low-dimensional antiferromagnets," Low Temp. Phys. **21**, 275–301 (1995).
[23]S. Komineas and N. Papanicolaou, "Vortex dynamics in two-dimensional antiferromagnets," Nonlinearity **11**, 265–290 (1998).
[24]E. G. Tveten, T. Müller, J. Linder, and A. Brataas, "Intrinsic magnetization of antiferromagnetic textures," Phys. Rev. B **93**, 104408 (2016).
[25]B. A. Ivanov, "Mesoscopic antiferromagnets: Statics, dynamics, and quantum tunneling (Review)," Low Temp. Phys. **31**, 635–667 (2005).
[26]E. Turov, *Physical Properties of Magnetically Ordered Crystals* (Academic Press, 1965).
[27]Y. M. Gufan, K. Kocharyan, A. Prokhorov, and E. Rudashevskii, "Dependence of the resonant frequencies of antiferromagnets on the magnetic field, and antiferromagnetic resonance in CoF_2," J. Exp. Theor. Phys. **39**, 565 (1974) [Zh. Exp. Teor. Fiz. **66**, 1155 (1989)]; available at http://www.jetp.ac.ru/cgi-bin/e/index/e/39/3/p565?a=list
[28]N. Papanicolaou, "Antiferromagnetic domain walls," Phys. Rev. B **51**, 15062–15073 (1995).
[29]"SLaSi spin–lattice simulations package" (unpulbished); see http://slasi.knu.ua/.
[30]D. D. Sheka, V. P. Kravchuk, and Y. Gaididei, "Curvature effects in statics and dynamics of low dimensional magnets," J. Phys. A **48**, 125202 (2015).
[31]O. V. Pylypovskyi, D. D. Sheka, V. P. Kravchuk, K. V. Yershov, D. Makarov, and Y. Gaididei, "Rashba torque driven domain wall motion in magnetic helices," Sci. Rep. **6**, 23316 (2016).
[32]O. M. Volkov, D. D. Sheka, Y. Gaididei, V. P. Kravchuk, U. K. Rößler, J. Fassbender, and D. Makarov, "Mesoscale Dzyaloshinskii-Moriya interaction: Geometrical tailoring of the magnetochirality," Sci. Rep. **8**, 866 (2018).
[33]D. D. Sheka, V. P. Kravchuk, K. V. Yershov, and Y. Gaididei, "Torsion-induced effects in magnetic nanowires," Phys. Rev. B **92**, 054417 (2015).
[34]V. V. Slastikov and C. Sonnenberg, "Reduced models for ferromagnetic nanowires," IMA J. Appl. Math. **77**, 220–235 (2012).
[35]A. A. Khajetoorians, J. Wiebe, B. Chilian, and R. Wiesendanger, "Realizing all-spin-based logic operations atom by atom," Science **332**, 1062–1064 (2011).
[36]S. Loth, S. Baumann, C. P. Lutz, D. M. Eigler, and A. J. Heinrich, "Bistability in atomic-scale antiferromagnets," Science **335**, 196–199 (2012).
[37]A. A. Khajetoorians, J. Wiebe, B. Chilian, S. Lounis, S. Blügel, and R. Wiesendanger, "Atom-by-atom engineering and magnetometry of tailored nanomagnets," Nat. Phys. **8**, 497–503 (2012).
[38]P. King, T. C. Stamatatos, K. A. Abboud, and G. Christou, "Reversible size modification of Iron and Gallium molecular wheels: A Ga_{10} 'Gallic wheel' and large Ga_{18} and Fe_{18} wheels," Angew. Chem., Int. Ed. **45**, 7379–7383 (2006).
[39]M. G. Sorolla, X. Wang, T. Makarenko, and A. J. Jacobson, "A large spin, magnetically anisotropic, octanuclear vanadium(iii) wheel," Chem. Commun. **55**, 342–344 (2019).
[40]"High–performance computing cluster of Taras Shevchenko National University of Kyiv," http://cluster.univ.kiev.ua/eng/.